An Analytical Model for Tropical Relative Humidity

DAVID M. ROMPS

Department of Earth and Planetary Science, University of California, Berkeley, and Earth Sciences Division,
Lawrence Berkeley National Laboratory, Berkeley, California

ABSTRACT

An analytical model is derived for tropical relative humidity using only the Clausius–Clapeyron relation, hydrostatic balance, and a bulk-plume water budget. This theory is constructed for radiative–convective equilibrium and compared against a cloud-resolving model. With some reinterpretation of variables, it can be applied more generally to the entire tropics.

Given four variables—pressure, temperature, and the fractional entrainment and detrainment rates—the equations predict the relative humidity (RH) and the temperature lapse rate analytically. The RH is a simple ratio involving the fractional detrainment rate and the water-vapor lapse rate. When integrated upward in height, the equations give profiles of RH and temperature for a convecting atmosphere.

The theory explains the magnitude of RH and the "C" shape of the tropospheric RH profile. It also predicts that RH is an invariant function of temperature as the atmosphere warms, and this behavior matches what has been seen in global climate models and what is demonstrated here with cloud-resolving simulations. Extending the theory to include the evaporation of hydrometeors, a lower bound is derived for the precipitation efficiency (PE) at each height: $PE > 1 - RH$. In a cloud-resolving simulation, this constraint is obeyed with the PE profile taking the shape of an inverted C shape.

1. Introduction

One of the most important problems in the study of climate change is to understand how the distribution of water vapor will change with warming. Water vapor is the atmosphere's most powerful greenhouse gas, and changes in its distribution can have significant implications for radiative forcing. A first step in predicting those changes is to develop theories for the distribution of water vapor in the current climate.

In this study, we endeavor to build an analytical model for the vertical distribution of water vapor in the tropics. The top panel of Fig. 1 shows the annual mean relative humidity at 500 hPa over the tropics, as diagnosed from the Interim European Centre for Medium-Range Weather Forecasts Re-Analysis (ERA-Interim) for the year 2013. The regions of high relative humidity (RH) coincide with regions with significant amounts of deep convection (i.e.,

the Indo-Pacific warm pool, the ITCZ, and equatorial Africa and South America). The region with the largest RH at 500 hPa in the annual mean is the Malay Archipelago, defined here as encompassing Indonesia, Malaysia, and Papua New Guinea. In Fig. 1, a box has been drawn around this region subjectively, extending from 6°S to 7°N and 85° to 155°E.

The bottom panels in Fig. 1 plot the mean profiles of RH over the entire tropics (dashed, defined here as the average over 20°S–20°N) and over the Malay Archipelago (solid, defined by averaging over the box depicted in the top panel). The mean profiles have been plotted in three different ways to be consistent with later figures. The three plots show the RH plotted as a function of height (left), pressure (center), and temperature (right). In the troposphere, we see that the RH profiles have a "C" shape, with local maxima at the bottom and top of the free troposphere (a relative humidity of about 80%– 90% for both) and a local minimum in the middle of the troposphere (about 30% for the entire tropics and about 60% for the Malay Archipelago).

There are some very basic questions that we can ask about these profiles. The following five questions will be addressed here.

Corresponding author address: David M. Romps, Department of Earth and Planetary Science, 377 McCone Hall, University of California, Berkeley, Berkeley, CA 94720.
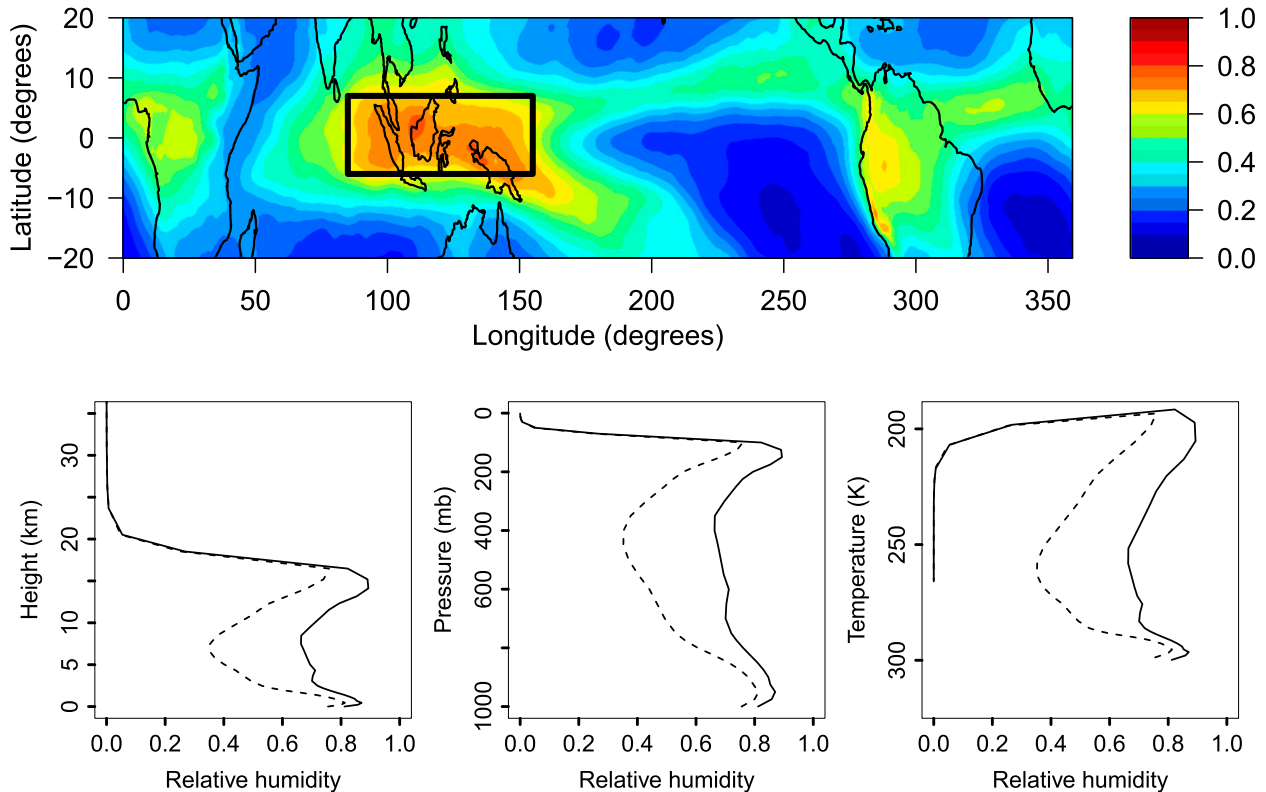E-mail: romps@berkeley.edu

FIG. 1. (top) Map of annual-mean relative humidity at 500 hPa in the tropics from ERA-Interim during the year 2013. (bottom) Mean profiles of relative humidity for the Indo-Pacific warm pool (solid; averaged over the black box in the top panel) and the entire tropical domain (dashed, 20°S–20°N) as a function of (left) height, (center) pressure, and (right) temperature.

1) Why does the RH profile take values in the range of 30%–90%? In other words, what basic physics prevents the RH from taking values near 1% or, at the other extreme, around 99%? Since relative humidity is a dimensionless quantity, its magnitude should be set by the dimensionless ratio of some physical constants. If we knew what the relevant physical constants were, then we could explain the 30%–90% range of RH.

2) Why is the tropospheric RH profile shaped like the letter C? As discussed below, this basic shape is ubiquitous in observations, global climate models, cloud-resolving models, and even simple numerical models. Therefore, a simple and robust mechanism must be responsible.

3) How should the free-troposphere RH change with warming? Since water vapor is the earth's dominant greenhouse gas, any future changes in RH would modulate the powerful water vapor feedback. It is typically assumed that the distribution of RH will be the same in a future climate as it is in the present climate, but what physics underlies such an assumption? In fact, GCMs do predict some changes in relative humidity, as shown in Fig. 2 of Sherwood et al. (2010a). As seen there, the multimodel mean exhibits an increase of RH over the lower half of the tropical troposphere, capped by a decrease in the tropical upper troposphere and an increase in the tropical lower stratosphere. These changes are interpreted by Sherwood et al. as an upward shift of the RH profile, but it remains to be understood what physics is responsible for such a shift.

4) What role does the evaporation of hydrometeors play in setting the relative humidity? It has been suggested that the RH profile in the tropics is set primarily by the evaporation of hydrometeors (Sun and Lindzen 1993, hereafter SL93). If true, this would suggest that the RH of the troposphere is not set by simple physics, but is set, instead, by complicated details of water microphysics. SL93 argue that, if warming increases the fraction of condensed water that reaches the ground as precipitation (i.e., as measured by an appropriate definition of precipitation efficiency), then the relative humidity should decrease, thereby weakening the water vapor feedback. A simple model for tropical RH would aid in exploring this proposed sensitivity to precipitation efficiency.

5) How is precipitation efficiency related to relative humidity? In the mechanism proposed by SL93, it is assumed that the precipitation efficiency increases with warming. If we can relate precipitation efficiency to relative humidity, then a theory for the latter should tell us something about the former. This might provide some guidance on what future changes to expect in tropical precipitation efficiency.

These five questions will be answered in sections 3 through 7, respectively.

Over the past two decades, there have been many studies that have simulated the RH over the entire tropics using reanalyzed winds and an advection–condensation model (e.g., Yang and Pierrehumbert 1994; Sherwood 1996; Pierrehumbert 1998; Galewsky et al. 2005; Dessler and Minschwaner 2007; Pierrehumbert et al. 2007; Sherwood et al. 2010b). In those numerical models, it is assumed that parcels of air get brought up to some relative humidity (e.g., 100%, or 90%) when they pass through a convecting region and that their relative humidity drops as they radiate energy and sink. Such simulations have had success in replicating the gross features of the RH distribution in the tropics.

There have also been efforts to replicate the tropical RH profile using simple numerical models in which subsiding air is treated as a steady plume whose RH is decreased by subsidence and increased by either the injection of saturated air from convecting regions or the evaporation of hydrometeors. SL93 present a numerical model for the tropical RH profile in which all of the moistening of subsiding air between 2 and 10 km is due to the evaporation of precipitation. Folkins et al. (2002, hereafter FKW02) and Minschwaner and Dessler (2004, hereafter MD04) use a one-dimensional, steady-state, bulk-plume model of the subsiding air, but assume that the air is moistened not by the evaporation of hydrometeors, but by the mixing in of air that diverges out of convecting regions.

None of these studies presents a complete and self-consistent model for tropical RH. The model of SL93 is based on the notion that no saturated parcel detrains from convection between 2 and 10 km, which is at odds with the known variety of convective outflow heights (e.g., Betts 1990). By omitting the detrainment of convection at all heights, their model biases the RH low, or requires an artificially large moistening by hydrometeors to compensate. The studies of FKW02 and MD04 both assume that the moistening of subsiding air is due only to detrainment from convection. Both of these studies make the same oversimplification, which is to define detrainment as $d = -\partial_z M$, where M is the convective mass flux. This neglects the fact that there is both

entrainment e and detrainment d at each height. The correct equation would be $d = e - \partial_z M$, which would give a higher detrainment rate and further weight the humidity toward the saturation humidity of nearby altitudes. In addition, both studies assume that the subsiding region gives *saturated* air to the convecting updrafts at heights where $\partial_z M > 0$; see Eqs. (1) and (2) of FKW02 and Eq. (3) of MD04 (also, note the sign error in that equation). By removing saturated air from the subsaturated subsidence regions, these equations overdry the subsiding air, again tending to bias the RH low. FKW02 makes an additional oversimplification: their Eq. (1) gives the humidity at a level as the average of saturation humidities at all levels above weighted by the detrainment rate. This is incorrect because some of the air from above the observation level gets entrained into updrafts before making it down to the observation level; therefore, their Eq. (1) gives too much weight to air from higher up, once again biasing the humidity low. As a consequence of all of these features, the model of FKW02 underestimates RH by an order of magnitude in the midtroposphere, as can be seen in their Fig. 3.

Despite these deficiencies and very different sets of assumptions, all three of these models succeed in replicating a ''C''-shaped RH profile. And, they are not alone. Cloud-resolving models of radiative–convective equilibrium also produce the C-shaped RH profile. See, for example, Fig. 11a of Held et al. (1993), Fig. 7 of Tompkins (2000), and Fig. 1 of Romps (2011). GCMs do it, too; see Fig. 1 of Sherwood et al. (2010a). The success that all of these different models have in generating a C-shaped RH profile suggests that the profile is set by some basic physics that is common to all these models and to the real atmosphere. But, what is that physics?

With regards to that question, Mapes (2001) provided a key piece of insight. He performed a calculation in which a column of atmosphere originally at saturation was allowed to cool radiatively and sink to maintain a constant temperature profile. His Fig. 2 shows an evolution of a C-shaped RH profile. At a height of 11 km, the radiative cooling and associated subsidence lead to a halving of the relative humidity in only one day. Mapes explains that this evolution is a consequence of the nearly dry-adiabatic lapse rates at those altitudes, which causes a large amount of subsidence (and, therefore, reduction in RH) for a given amount of radiative cooling. At much higher and lower altitudes, the lapse rate is not as steep, causing a smaller reduction in RH for the same cooling.

What is missing from that time-dependent picture is some process for moistening the air, which would allow for a steady-state profile. In the model of Sherwood et al. (2006, hereafter SKR06), the moistening that balances

this drying is parameterized as a Poisson process: each parcel of air has a fixed probability per time of being instantaneously moistened back to saturation, with a mean time between saturation events chosen to be a constant 7 days. The competition between this 7-day moistening and the lapse-rate- and radiative-cooling-rate-dependent drying leads to a C-shaped profile. Basically, we can think of this approach as taking the drying tendencies calculated by Mapes (2001) and multiplying them by a 7-day time scale. SKR06 imagines the 7-day time scale to be the typical time for an air parcel to make contact with a convecting region. The idea is that a parcel descends, occasionally gets moistened in situ, and continues on its way. But, this is not how the atmosphere works. In order for a parcel to get moistened, it must participate in convection or evaporate precipitation, and either process will move the parcel rapidly to another altitude. Nevertheless, we will see in section 8 how to give a physical interpretation to the moistening time scale of SKR06.

2. Theory

The goal of this section is to derive an analytic theory for relative humidity in a convecting atmosphere. This theory is not intended as a substitute for numerical simulations with a global climate model or a cloud-resolving model (CRM). Instead, it is intended as a distillation of the essential processes responsible for setting relative humidity, and the ambition is to gain physical insight into their workings. For the sake of simplicity, we will construct this theory for radiative–convective equilibrium (RCE). In RCE, the net heating from moist convection is in balance with the net radiative cooling, and there are no large-scale winds. Although, strictly speaking, RCE does not exist anywhere in the tropics, it is considered a prototype for the real convecting atmosphere and is often used as a simple analog for the deeply convecting tropics. As we will discuss in section 8, it will be possible to broaden our interpretation of the theoretical parameters to apply the theory more broadly to the tropics and subtropics as a whole.

To make this theory analytically solvable, three primary approximations must be made. The first of these is to treat convection as an entraining/detraining bulk plume. In this simplification, convecting clouds have a single set of thermodynamic properties at each altitude (e.g., Malkus 1952; Schneider and Lindzen 1976; Romps 2012). It is known, in fact, that clouds are quite heterogeneous at each level (e.g., Paluch 1979) and that this heterogeneity is generated by a spectrum of entrainment rates (Arakawa and Schubert 1974; Romps and Kuang 2010a, b), but a single plume with a single profile of

entrainment rate has still had some success in modeling convection (de Rooy et al. 2013). The second approximation is to treat condensates as precipitating out of the atmosphere immediately upon formation. Physically, this may be thought of as the condensates having an infinite free-fall speed. For the time being, this eliminates the possibility of atmospheric moistening by evaporating precipitation, but we will come back to this effect—and account for it—in section 6. The third approximation is to treat the convecting plume as having the same temperature as its environment. Neglecting virtual effects, this is tantamount to enforcing zero buoyancy for convection. This approach is motivated by the work of Singh and O'Gorman (2013), who showed from cloud-resolving simulations that this is a decent approximation over a wide range of climates.

a. Saturation specific humidity q_v^*

Throughout this derivation, we will denote the water vapor mass fraction in the nonconvecting environment by q_v. Since convection occupies a small fractional area in RCE, $q_v(z)$ also represents the specific humidity averaged over the entire area at height z. Therefore, we will interchangeably refer to q_v as the specific humidity of the environment and of the entire atmosphere. Since we are approximating convection as having no condensates (due to the infinitely fast free-fall speed) and the same temperature as the environment, the total water mass fraction of clouds at height z is simply equal to the environment's saturation humidity, which we denote by $q_v^*(z)$.

The first step in our derivation is to obtain an expression for the height dependence of $q_v^*(z)$ in terms of temperature and the temperature lapse rate. By the Clausius–Clapeyron relation, the saturation vapor pressure, which we will denote by p_v^*, is related to temperature by

$$p_v^* \sim e^{-L/R_v T}, \qquad (1)$$

where L is the latent heat of evaporation, R_v is the specific gas constant of water vapor, T is the air temperature, and the tilde denotes an approximate proportionality. For simplicity, we will ignore the latent heat of melting; it can be accounted for in the final equations by considering L to be the sum of the two latent heats at temperatures sufficiently below freezing. Taylor expanding $1/T$ to first order in $z - z_0$ around height z_0, we get

$$p_v^* \sim e^{-L\Gamma(z-z_0)/R_v T^2}, \qquad (2)$$

where Γ is the temperature lapse rate.

Next, the saturation mass fraction q_v^* is related to p_v^* by

$$q_v^* \sim \frac{p_v^*}{p}, \tag{3}$$

where p is the total atmospheric pressure. We can approximate p around height z_0 as

$$p \sim e^{-g(z-z_0)/R_a T}, \tag{4}$$

where g is the gravitational acceleration and R_a is the specific gas constant of dry air (i.e., ignoring the virtual effect of water vapor). By combining Eqs. (2)–(4), we obtain

$$q_v^*(z) = q_v^*(z_0)e^{-\gamma(z-z_0)}, \tag{5}$$

where the water-vapor lapse rate γ is given by

$$\gamma = \frac{L\Gamma}{R_v T^2} - \frac{g}{R_a T}, \tag{6}$$

with T and Γ evaluated at z_0. This water-vapor lapse rate will play a leading role in the ensuing theory. Note that γ is a function only of fundamental constants (L, g, R_v, and R_a) and of T and Γ.

b. Relative humidity

To derive an expression for RH, we will begin with the bulk-plume equations for convection and its environment. Let M denote the convective mass flux (units of $kg\,m^{-2}\,s^{-1}$), e and d denote the entrainment and detrainment rates (units of $kg\,m^{-3}\,s^{-1}$), and c denotes the condensation rate (units of $kg\,m^{-3}\,s^{-1}$). We can then write down the following equations for the steady-state convective mass flux M, the humidity within clouds q_v^*, and the humidity within the environment q_v:

$$\partial_z M = e - d, \tag{7}$$

$$\partial_z(Mq_v^*) = eq_v - dq_v^* - c, \quad \text{and} \tag{8}$$

$$\partial_z(-Mq_v) = dq_v^* - eq_v. \tag{9}$$

Since M is the total mass flux and q_v is a mass fraction (as opposed to a mixing ratio), there should technically be a $-c$ on the rhs of Eq. (7). For small q_v^*, as in the earth's atmosphere, this term has a negligible impact and its inclusion greatly complicates the equations, so it has been omitted. Defining the fractional entrainment and detrainment rates as $\varepsilon = e/M$ and $\delta = d/M$, the mass flux M can be eliminated from these equations to yield

$$\partial_z q_v^* = \varepsilon(q_v - q_v^*) - c/M, \tag{10}$$

$$-\partial_z q_v = \delta(q_v^* - q_v). \tag{11}$$

Let us focus first on Eq. (11), which gives the vertical gradient of environmental humidity. Writing q_v as RHq_v^* and using Eq. (5), Eq. (11) can be written as

$$RH\gamma - \partial_z RH = \delta(1 - RH).$$

Assuming that RH varies over distances that are large compared to the characteristic distance of variations in q_v^*, the second term on the left-hand side can be approximated as zero, and this simplifies to

$$RH = \frac{\delta}{\delta + \gamma}. \tag{12}$$

Note that $1/\delta$ is the length scale over which convection moistens the environment toward saturation, and $1/\gamma$ is the length scale over which subsidence drives RH toward zero. The relative humidity is set by the balance between these two processes. If δ is large, then the moistening effect of convection wins out over subsidence-driven drying, and RH is near unity. If δ is small, then the moistening effect of convection is small—operating over very large distances—which allows the subsidence-driven drying to dominate; therefore, RH is near zero.

c. Condensation rate c

Let us briefly consider the condensation rate c. Equation (10) can be written as

$$c = [\gamma - \varepsilon(1 - RH)]Mq_v^*. \tag{13}$$

In order for c to be positive, the right-hand side must be positive, which places the following constraint on RH:

$$RH > 1 - \gamma/\varepsilon. \tag{14}$$

Convective clouds, which require positive condensation, can exist only when this inequality is satisfied. To write this in a more illuminating form, we can replace RH using Eq. (12) and then use Eq. (7) to find

$$\partial_z M < \gamma M. \tag{15}$$

In other words, moist convection is possible so long as the convective mass flux does not increase with height too rapidly. In fact, convective mass fluxes typically decrease with height, so this constraint is satisfied.

d. Temperature lapse rate Γ

Next, let us derive the temperature lapse rate. The moist static energy of the environment is given by $h = c_p T + gz + Lq_v$, while that of the cloud is given by

$h^* = c_p T + gz + Lq_v^*$. Using Eqs. (5) and (6), $\partial h^*/\partial z$ is found to be

$$\partial_z h^* = g\left(1 + \frac{q_v^* L}{R_a T}\right) - \Gamma\left(c_p + \frac{q_v^* L^2}{R_v T^2}\right). \quad (16)$$

By writing down the steady-state budget of moist static energy for the convection, we can obtain a second equation for $\partial_z h^*$. The steady-state budget is given by $\partial_z(Mh^*) = eh - dh^*$. Using Eq. (7), this can be written as $\partial_z h^* = \varepsilon(h - h^*)$. Since $h - h^* = L(q_v - q_v^*) = L(\mathrm{RH} - 1)q_v^*$, Eq. (12) can be used to arrive at

$$\partial_z h^* = -\varepsilon L q_v^* \frac{\gamma}{\delta + \gamma}. \quad (17)$$

Equating the right-hand sides of Eqs. (16) and (17), we get an expression for Γ:

$$\Gamma = \frac{g\left(1 + \frac{q_v^* L}{R_a T}\right) + q_v^* L \frac{\varepsilon \gamma}{\delta + \gamma}}{c_p + \frac{q_v^* L^2}{R_v T^2}}. \quad (18)$$

This is an implicit equation for Γ since γ depends on Γ through Eq. (6). Writing Γ in terms of γ using Eq. (6), we get

$a_1 \gamma^2 + a_2 \gamma + a_3 = 0,$ where

$$a_1 = \frac{R_v c_p T^2}{L} + q_v^* L > 0,$$

$$a_2 = \frac{R_v c_p T^2}{L}\left(\delta + \frac{g}{R_a T}\right) + q_v^* L(\delta - \varepsilon) - g, \quad \text{and}$$

$$a_3 = \left(\frac{R_v c_p T}{R_a L} - 1\right)g\delta < 0.$$

Note that the sign of a_2 is variable, but a_1 is always positive and a_3 is always negative. In terms of these constants, Γ is given by

$$\Gamma = \frac{R_v T^2}{L}\left(\frac{-a_2 + \sqrt{a_2^2 - 4a_1 a_3}}{2a_1} + \frac{g}{R_a T}\right). \quad (19)$$

Equation (19) gives Γ as a function only of physical constants (c_p, R_v, R_a, g, and L) and of pressure, temperature, and the fractional entrainment/detrainment rates (p, T, ε, and δ). Since Eq. (12) was used in the derivation of this equation, this expression for Γ accounts for the coupled relationships between the relative humidity, the impact of RH on the lapse rate through entrainment, and the effect of lapse rate on the relative humidity through detrainment. To calculate RH, we need only to substitute this value of Γ into Eq. (6) to get γ and then use γ in Eq. (12) to get RH. Therefore, Eqs. (12) and (19) form the analytical model that we sought: given the pressure p, temperature T, entrainment rate ε, and detrainment rate δ at some height in the atmosphere, this theory gives Γ and RH at that height.

Figure 2 plots the predicted RH at a temperature of 300 K and pressure of 1 bar (1 bar = 1000 hPa) over a range of fractional entrainment and detrainment rates. To aid the eye, the dashed line denotes $\varepsilon = \delta$ (i.e., the points corresponding to a mass flux that is constant with height). The white region covers the values of ε and δ that violate the inequality in Eq. (15), where moist convection is not possible. Note that, at fixed ε, RH increases with increasing δ. Mathematically, this is an obvious consequence of Eq. (12). Physically, the increase in detrainment moistening leads to a higher steady-state humidity. On the other hand, at fixed δ, an increase in ε leads to a decrease in RH. This occurs because, at a higher entrainment rate, the atmosphere must have a higher Γ to permit moist convection. This, in turn, increases the water-vapor lapse rate γ, which enhances the subsidence drying; mathematically, the increase in γ lowers RH in Eq. (12). If we increase both ε and δ by the same amount, this increases the cloud–environment exchange without changing $\partial_z M$, and it moves us up a one-to-one line in Fig. 2. This equal increase in ε and δ leads to an increase in RH: the increase in detrainment moistening wins out over the increase in subsidence drying caused by the steepened lapse rate.

Figure 3 plots the predictions for $\partial \mathrm{RH}/\partial T$ at $T = 300$ K and $p = 1$ bar while holding p, ε, and δ constant. The first thing to note is that all of the values are positive: the theory predicts $\partial \mathrm{RH}/\partial T > 0$. The largest increase in RH occurs for $\varepsilon = 0$ and $\delta = 0.1$ km^{-1}, where $\partial \mathrm{RH}/\partial T = 0.012$ K^{-1} (i.e., a 1-K warming would increase RH from 50.0% to 51.2%). Typical values for ε and δ in the earth's atmosphere are $\delta > \varepsilon$ and 0.2 km$^{-1} < \delta < 2$ km^{-1}. For these values, $\partial \mathrm{RH}/\partial T$ lies in the range of about 0.003–0.008 K^{-1}. For example, a relative humidity of 80.0% at 300 K would increase to somewhere in the range of 80.3%–80.8% at 301 K depending on the values of ε and δ.

3. The physics behind a relative humidity of 30%–90%

With Eq. (12) for RH, we can answer question number 1 posed in the introduction: why is RH on the order of 30%–90% and not, say, 1% or 99%? A typical value for the fractional detrainment rate δ is around 2 km^{-1} for shallow convection (e.g., Siebesma and Cuijpers 1995; Romps 2010) and perhaps as low as 0.2 km^{-1} for deep
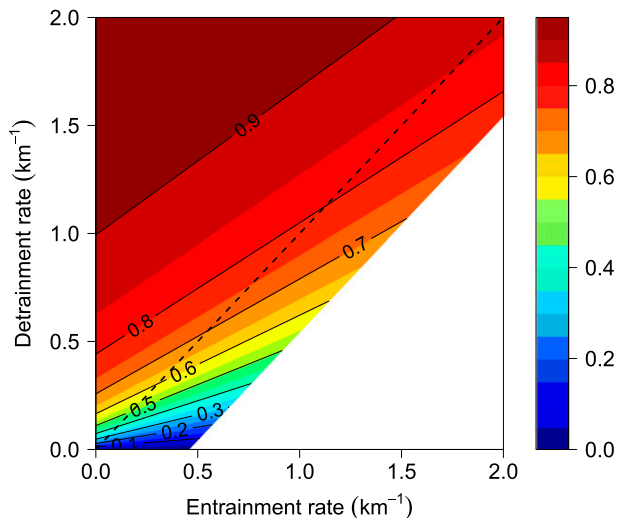
FIG. 2. Theoretical prediction for RH at $T = 300\,\mathrm{K}$ and $p = 1\,\mathrm{bar}$, as a function of entrainment rate (abscissa) and detrainment rate (ordinate). The dashed line denotes $\varepsilon = \delta$, where the mass flux is constant with height. The white region corresponds to values of ε and δ for which moist convection is not possible.

FIG. 3. As in Fig. 2, but for $\partial \mathrm{RH}/\partial T$ (K^{-1}) at $T = 300\,\mathrm{K}$, $p = 1\,\mathrm{bar}$ and holding p, ε, and δ constant.

convection (e.g., Romps 2010; Böing et al. 2012). Substituting $T = 300\,\mathrm{K}$ and $\Gamma = 6.5\,\mathrm{K\,km}^{-1}$ into Eq. (6), we find that a typical value for the water-vapor lapse rate γ is $0.3\,\mathrm{km}^{-1}$. Consequently, Eq. (12) tells us that RH should range from about $0.2/(0.2 + 0.3) = 40\%$ to $2/(2 + 0.3) = 90\%$. These rough numbers agree well with the range of about 30%–90% seen in the observations of Fig. 1.

Furthermore, it is clear why free-tropospheric RH cannot be 1% or 99% in the presence of convection. For RH to be 1%, δ would need to equal 0.01 times γ, which would be $0.003\,\mathrm{km}^{-1}$. In other words, clouds would entrain only a few percent of their original mass as they rise through the depth of the troposphere. It is well known that deep convection is unable to sustain such undiluted ascent in the earth's current atmosphere (e.g., Kuang and Bretherton 2006; Romps and Kuang 2010a; Fierro et al. 2012). To support such undiluted ascent, the atmosphere would need to have a well-isolated patch of convection, akin to what is seen in simulations of convective aggregation with no wind shear (Held et al. 1993; Bretherton et al. 2005). In the presence of shear, waves, and large-scale circulations, such an extreme case of convective aggregation is an unlikely outcome for the current climate or other nearby climate states.

For RH to be 99%, δ would need to equal 100 times γ, which would be $30\,\mathrm{km}^{-1}$. To avoid rapid extinction of convective mass fluxes with height, the fractional entrainment rate would need to be comparable. The resulting convection would entrain and detrain environmental air so rapidly that the net effect would be an effective diffusivity.
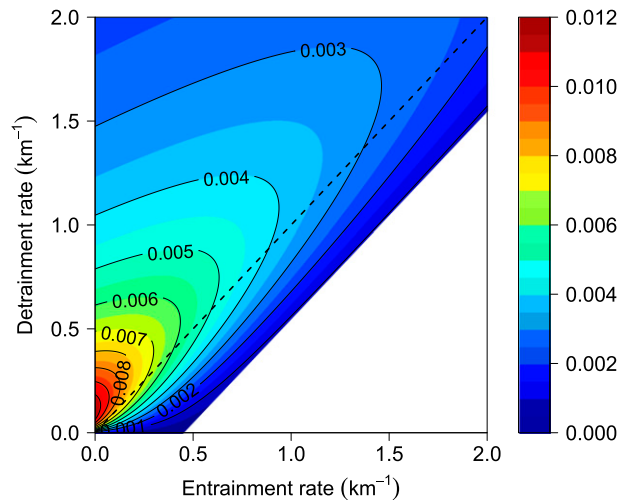
Physically, this could be pictured as a nearly saturated atmosphere filled with small-scale eddies causing local drying by condensation, which is balanced by an upward diffusion of water vapor. Such a state would require the convecting eddies to be distributed uniformly throughout the atmosphere. To generate such a state over the entirety of the tropical oceans, we would need a uniform sea surface temperature and a uniform Coriolis parameter, neither of which are possible on a spherical, rotating planet. So, we can safely rule out a relative humidity of 99% throughout the troposphere in the earth's current or nearby climate states.

4. The C shape of RH explained

To understand the C shape of the RH profile, we need to study Eqs. (6) and (12), which give the expressions for γ and RH. As we move upward in the troposphere, γ increases because the growth in its first (positive) term outpaces the growth in its second (negative) term. The first term grows because Γ increases with height (i.e., a steeper lapse rate at higher altitudes) and T^2 decreases with height. This increase in γ tends to cause RH to decrease since $\mathrm{RH} = \delta/(\delta + \gamma)$. For RCE, the detrainment rate δ is approximately constant or decreasing with height in the lower and middle troposphere; see the right panel of Fig. 7 of Romps (2010) and Fig. 6 of Romps (2014). Any decrease in δ will also tend to decrease RH. Therefore, we see that the altitude dependence of γ and δ in the lower half of the troposphere both favor $\partial_z \mathrm{RH} < 0$.

In the upper half of the troposphere, γ can be approximated by the first term on the rhs of Eq. (6) with Γ replaced by g/c_p, which gives $\gamma = Lg/(c_p R_v T^2) \approx 1\,\mathrm{km}^{-1}$.

The important conclusion from this is that γ is finite in the upper troposphere. Meanwhile, δ is not finite, but goes toward infinity as we move upward toward the height where the mass flux goes to zero. This can be seen from the mass budget: $\partial_z M = (\varepsilon - \delta)M$, which can be written as $\delta = \varepsilon - \partial_z M/M$. No matter how M goes to zero at the top of convection z_0, $\partial_z M/M$, and therefore δ, will go to infinity as $1/(z_0 - z)$. Since $RH = \delta/(\delta + \gamma)$, RH must increase with height in the upper troposphere toward one.

Putting it altogether, we see that the increasing γ and decreasing δ in the lower troposphere cause RH to decrease with height there. In the upper troposphere, the nearly constant γ and increasing δ cause RH to increase with height. Therefore, RH takes its lowest values in the middle troposphere, giving the RH profile its characteristic C shape.

5. An invariant RH–*T* curve with warming

Equation (19) has an important implication for climate change: holding the entrainment and detrainment rates constant, Eq. (19) predicts that Γ is, to good approximation, a function only of temperature, rather than a function of both temperature and pressure. There is some pressure dependence in q_v^*, but appendix A shows the effect of this dependence to be small. Equation (6) tells us that γ is a function only of temperature and Γ, so γ is also a function of temperature only. By Eq. (12), this implies that RH is a function only of temperature. In other words, as the troposphere warms or cools, the relative humidity is given by an invariant RH–*T* curve. Our next task is to calculate this curve.

a. *Theoretical* RH *profiles*

So far, we have used Eqs. (6), (12), and (19) to specify Γ and RH at a given p and T. But, we can also use these equations to construct entire profiles of temperature and humidity. Given surface values for p and T, we can integrate them upward in height using $dT = -\Gamma dz$ and $dp = -\rho g dz$. With those p and T profiles, we can then use Eq. (12) to find the profile of RH. Of course, we also need ε and δ for these calculations. Since ε, δ, and M are related by $\partial_z M/M = \varepsilon - \delta$, we can fulfill this requirement by specifying an entrainment rate, which we will choose to be a constant, and a profile of M. For the entrainment rate, we will use $\varepsilon = 0.5\,\mathrm{km}^{-1}$. We choose a constant value here for simplicity, and a value of $0.5\,\mathrm{km}^{-1}$ is chosen because it sits in between the smaller entrainment rates inferred for deep convection (e.g., Romps 2010; Böing et al. 2012; Romps 2014) and the larger rates inferred for shallow convection (e.g., Siebesma and Cuijpers 1995; Romps 2010; Romps and Kuang 2010b).

For the mass flux, we will construct a profile of M with three layers: the lower troposphere (in which the convective mass flux is constant with height), the upper troposphere (in which the mass flux decreases toward zero), and the stratosphere (in which $M = 0$ and both q_v and $\partial T/\partial z$ are constant with height). In particular, we use

$$M(z) \propto \begin{cases} 1, & z \leq h_1 \\ \dfrac{1}{2} + \dfrac{1}{2}\cos\left(\pi\dfrac{z - h_1}{h_2 - h_1}\right), & h_1 < z < h_2 \,, \\ 0, & z \geq h_2 \end{cases} \quad (20)$$

where $z = h_1$ is the top of the lower troposphere and $z = h_2$ is the top of the upper troposphere. In the lower troposphere, the constant mass flux is achieved by setting $\delta = \varepsilon$. As stated above, a value of $\varepsilon = 0.5\,\mathrm{km}^{-1}$ is used throughout the troposphere. In the upper troposphere, the mass flux is tapered to zero by increasing δ according to

$$\delta = \varepsilon + \frac{\pi}{h_2 - h_1}\frac{\sin[\pi(z - h_1)/(h_2 - h_1)]}{1 + \cos[\pi(z - h_1)/(h_2 - h_1)]}.$$

The height h_1, which separates the lower and upper troposphere, is chosen to be the height where T first reaches 240 K. This choice for a temperature-dependent detrainment layer is motivated by the hypothesis for a fixed anvil temperature (i.e., that the location of convective detrainment will occur at a fixed temperature as the atmosphere warms). Since first proposed by Hartmann and Larson (2002), this fixed-anvil-temperature (FAT) hypothesis has been demonstrated in cloud-resolving models (Kuang and Hartmann 2007; Harrop and Hartmann 2012). The depth of the detrainment layer is chosen to be $h_2 - h_1 = 7\,\mathrm{km}$, which sets h_2. The temperature in the stratosphere is chosen to be continuous with the temperature in the troposphere and to have a constant dT/dz of $1\,\mathrm{km}^{-1}$. The q_v in the stratosphere is taken as the value at the tropopause, as is approximately true in the tropical stratosphere due to the Brewer–Dobson circulation. The surface pressure is chosen to be 1 bar. Figure 4 summarizes all of these inputs to the theory.

The top panels of Fig. 5 show two profiles of temperature and relative humidity using these inputs. (The bottom panels, which include some reevaporation of condensates in the environment, will be discussed in section 6.) The solid profiles correspond to a surface temperature of 300 K, while the dashed curves correspond to a surface temperature of 310 K. Note that there is no subcloud layer in this theory, nor information
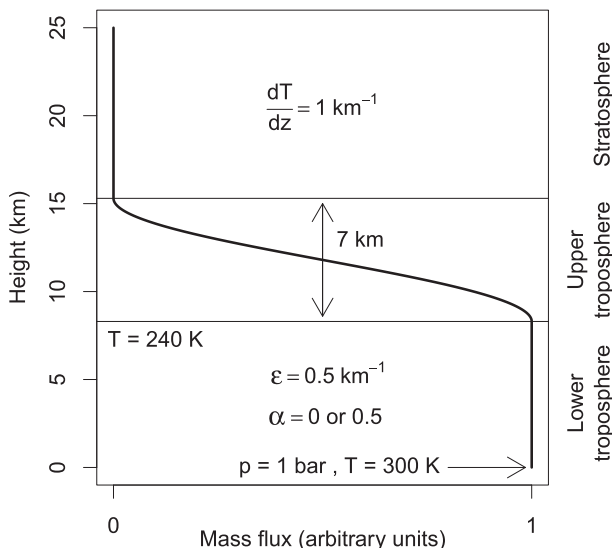
FIG. 4. The parameters provided to the theory to generate profiles of temperature and relative humidity.

about an air–surface temperature jump, so a more accurate interpretation of these "surface temperatures" is as the air temperature at cloud base. A subcloud layer and air–surface temperature jump could be added to the theory with ease, but they are not relevant for our purposes, so they are omitted for simplicity.

There are several notable features in the top panels of Fig. 5. We see that the RH profile has the characteristic C shape, and that RH peaks at unity at the top of the troposphere. Both of these features are explained in section 4. In the real atmosphere, the upper-tropospheric RH curve is rarely as spiked as is seen here. This is because the tropics have deep convection that terminates at a variety of different heights depending on location (e.g., western vs eastern Pacific) and time (e.g., due to diurnal cycles, seasonal cycles, and gravity waves). These different regions and times detrain air with a unit relative humidity at different heights, and mixing leads to an averaging, and therefore smoothing, of the different upper-tropospheric spikes.

Comparing the 300- and 310-K profiles in Fig. 5, it is evident that temperature increases more rapidly at fixed height in the upper troposphere than it does in the lower troposphere. This is the behavior expected for undiluted convection (i.e., a moist adiabat), and here we see that it also occurs for entraining convection. Comparing the solid and dashed curves at fixed heights, warming causes RH to increase in the lower and middle troposphere, decrease in the upper troposphere, and increase in the lower stratosphere. This is the same pattern of tropical $\partial RH/\partial T$ found by Sherwood et al. (2010a) in their analysis of global climate models (see their Fig. 2), where the

change in RH with warming is described as an upward shift.

What is the physical origin for this upward shift? The answer lies in the existence of an invariant RH–T curve, as discussed in the beginning of this section. Since RH is a function primarily of temperature, the profile of RH will shift upward with warming to stay on the RH–T curve. This behavior is illustrated in Fig. 6, which plots the theoretical RH profiles for surface temperatures of 290, 300, 310, and 320 K. The left and center panels plot these RH profiles as functions of height and pressure, respectively. Clearly, there are significant changes in RH with atmospheric warming both at constant height and at constant pressure. The right panel, however, shows the RH profiles plotted as a function of temperature. Plotted in this way, the RH profiles collapse onto an invariant RH–T curve.

b. CRM results

To find out if cloud-resolving simulations of RCE exhibit an invariant RH–T curve with warming, RCE simulations were run with Das Atmosphärische Modell (DAM) (Romps 2008). Simulations were run on a square doubly periodic domain with a width of 32 km and a model top at 61 km, and using a horizontal grid spacing of 2 km and a vertical grid spacing that varied smoothly from 50 m in the boundary layer to 500 m at a height of 5 km and to 1 km at 50 km. The time step alternated between 10 and 20 s depending on the Courant–Friedrichs–Lewy (CFL) condition. The lower boundary was specified to be an ocean surface with a fixed temperature, and surface fluxes were calculated using a bulk formula. Both shortwave and longwave radiation were calculated interactively using the Rapid Radiative Transfer Model (Clough et al. 2005; Iacono et al. 2008), and the top-of-atmosphere insolation was specified to be a constant diurnal average for the equator on 1 January. To prevent deviations from FAT due to an artificially fixed profile of ozone (Harrop and Hartmann 2012), the ozone profile has been set to zero. The microphysics was a six-class Lin–Lord–Krueger scheme (Lin et al. 1983; Lord et al. 1984; Krueger et al. 1995). Each simulation was equilibrated to RCE over 425 days, with averages taken over the last 30 days.

Figure 7 displays the RH profiles from runs with four SSTs—290, 300, 310, and 320 K—plotted as functions of height (left), pressure (center), and temperature (right). Plotted as a function of height and pressure, the RH profiles appear to shift upward with warming. For example, note the large upward shift in the tropospheric RH minimum: it moves from 5 to 15 km as SST increases from 290 to 320 K. When plotted against temperature, however, the RH profiles approximately collapse onto
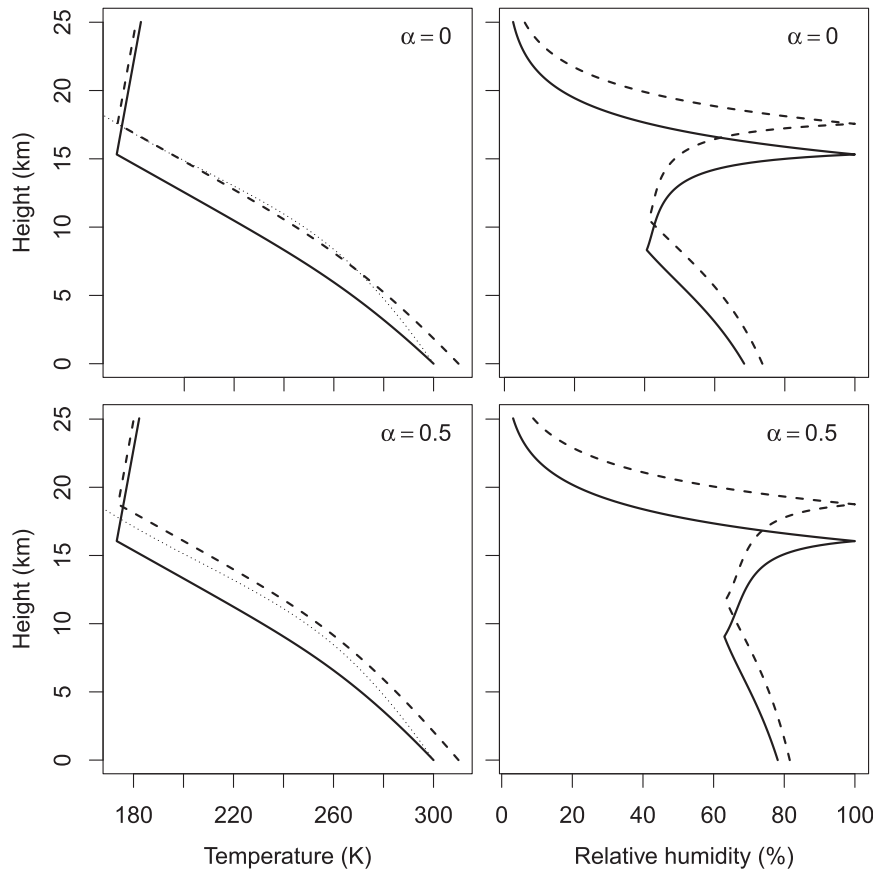
FIG. 5. Theoretical (left) temperature and (right) relative humidity profiles for surface-air temperatures equal to (solid) 300 and (dashed) 310 K. (top) The temperature and relative humidity profiles for a precipitation efficiency of 100% ($\alpha = 0$) (i.e., no evaporation of condensates in the environment). The dotted curve gives the temperature profile for a saturated parcel lifted pseudoadiabatically from the surface for the 300-K case. (bottom) As in the top panel, but for a precipitation efficiency of 50% ($\alpha = 0.5$).

a common curve. For example, note that the tropospheric RH minimum consistently occurs at a temperature of about 260 K. Despite a 30-K range in SST, the cloud-resolving simulations exhibit the same behavior as the theory: the RH profiles collapse onto an invariant RH–T curve.

To check the effect of grid spacing and domain size, the simulations were restarted on a larger horizontal domain (72 km × 72 km) with a finer horizontal grid spacing (500 m). These higher-resolution simulations were run for 60 days and the profiles were averaged over the last 30 days. The resulting profiles of relative humidity, shown in Fig. 8, are largely unchanged, although there is some additional spread in the midtroposphere RH minima. A possible explanation for the additional deviation from an invariant RH–T curve is that the higher resolution (16 times more grid points per horizontal area) allows for more subplume variability, causing deviations from the bulk-plume theory.

c. Why RH $\rightarrow 1$ as $T \rightarrow \infty$

An interesting feature seen in both theory and simulations is the increase of RH with increasing temperature. This can be seen from the slope of the RH profile at warm temperatures in the right panels of both Figs. 6, 7, and 8: the RH curve increases toward unity as the temperature increases.

Why does the atmosphere approach saturation as the temperature increases? We can understand the reason as follows. At high temperatures, the temperature lapse rate approximately asymptotes to a constant; for large T, the moist-adiabatic lapse rate goes to $\Gamma \approx gT/L \approx 1 \, \text{K km}^{-1}$. This implies that the amount of latent heat that clouds must release asymptotes to a constant amount per vertical distance (i.e., $\partial_z q_v^* \sim \text{constant}$). Meanwhile, q_v^* grows rapidly with temperature by the Clausius–Clapeyron relation, so the water-vapor lapse rate γ, which equals $-\partial_z q_v^*/q_v^*$, decreases rapidly with temperature. Since the
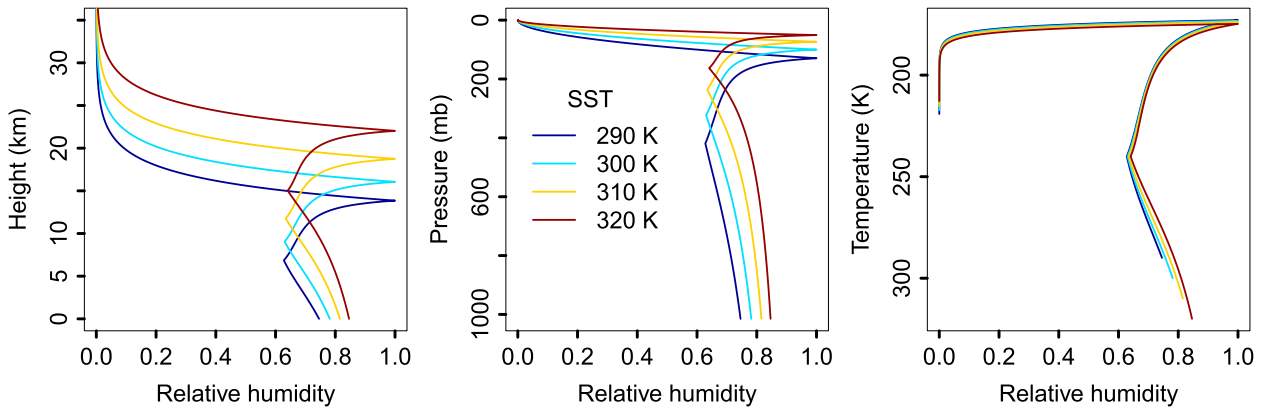
FIG. 6. Profiles of RH from theory for SST = 290, 300, 310, and 320 K and $\alpha = 0.5$ plotted as functions of (left) height, (center) pressure, and (right) temperature. Note the large changes in RH at constant height and constant pressure, but the invariance of RH at constant temperature. The profiles in the right panel collapse onto an invariant RH–T curve.

q_v at height z is roughly equal to the q_v^* detrained at height $z + 1/\delta$, the relative humidity is given by the ratio of the two. In other words, RH is approximately given by $q_v^*(z + 1/\delta)/q_v^*(z)$. For small γ/δ, we can Taylor expand this around z to get RH $\approx 1 - \gamma/\delta \approx \delta/(\delta + \gamma)$, which connects back to the exact expression given in Eq. (12). So, we see that RH is driven toward one as γ decreases with warming. Physically, this occurs because the air at height z has $q_v(z) = q_v^*(z + 1/\delta)$, which is increasingly similar to $q_v^*(z)$.

6. The effect of evaporating condensates

Up until now, we have assumed that condensates fall out of the atmosphere immediately upon formation. With this assumption, the mass fraction of condensates in updrafts q_c is identically zero, and the total-water mass fraction of updrafts is simply q_v^*. This leads to the steady-state equation for the environment's water budget, which was given in Eq. (11) and is also replicated here:

$$-\partial_z q_v = \delta(q_v^* - q_v). \qquad (21)$$

In the upper troposphere, however, the assumption of zero q_c is woefully violated. In fact, q_c can be larger than q_v^* by many multiples. This fact sounds like it would invalidate all of the preceding derivations and conclusions, but it does not. Accounting for condensates introduces a correction to Eq. (12) for the relative humidity, but does not alter the main conclusions.

If condensates do not fall out of updrafts immediately, what is their impact on the environmental humidity? Naively, we might try to modify the environment's water budget to include the detrainment of condensates as follows:

$$-\partial_z q_v = \delta(q_v^* + q_c - q_v) \quad (\text{incorrect!}). \qquad (22)$$

As indicated in parentheses above, this would be incorrect. The fatal error in this equation is its omission of hydrometeor fallout. In particular, it erroneously assumes
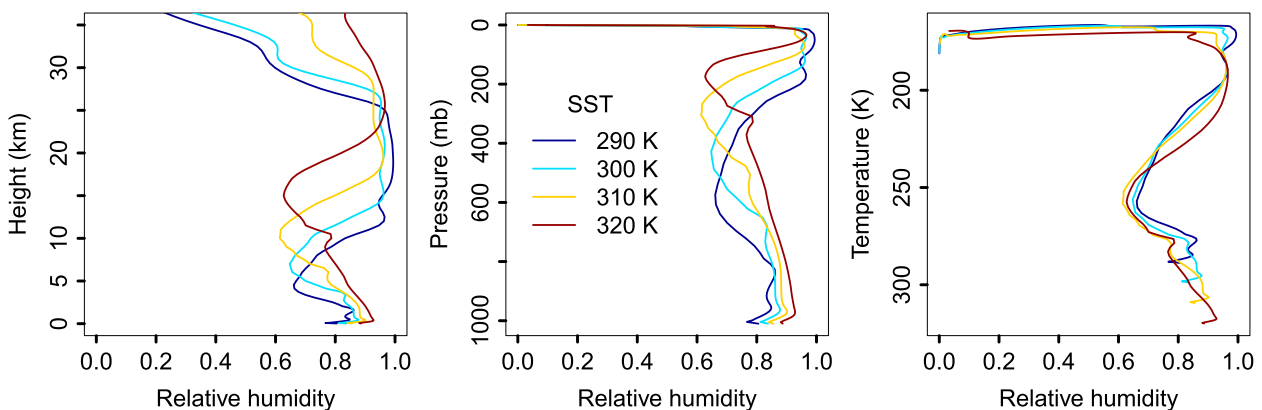

FIG. 7. Profiles of RH from cloud-resolving simulations with SST = 290, 300, 310, and 320 K and a grid spacing of 2 km. There is no ozone in these simulations.
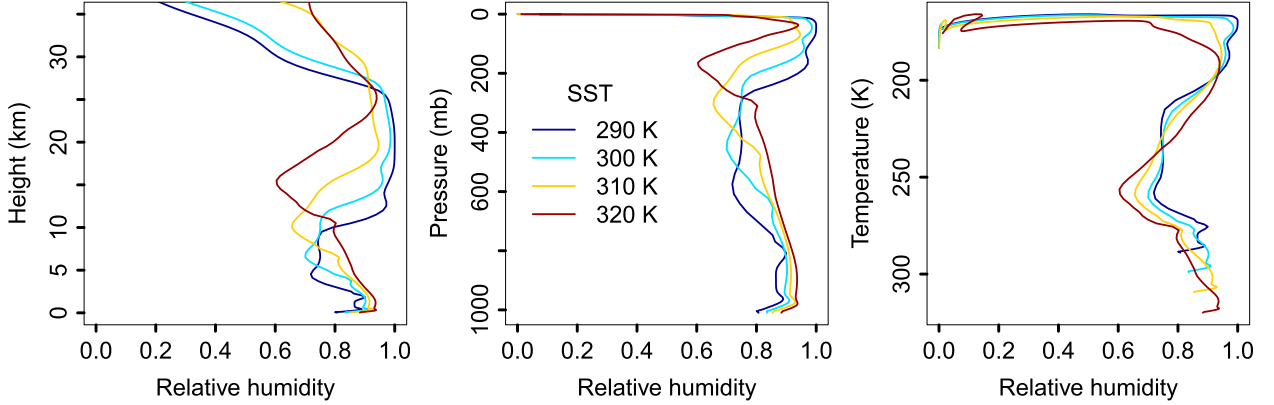
FIG. 8. As in Fig. 7, but for a finer grid spacing (500 m) and a larger domain (72 km × 72 km).

that the only way for condensates to exit an updraft is to exit with detrained cloud (as opposed to falling out of the updraft due to their finite terminal velocity) and that hydrometeors in detrained cloud evaporate into the environment at that height (as opposed to falling out and either evaporating at lower levels or reaching the surface as precipitation). By omitting fallout, Eq. (22) would grossly overestimate the moistening of the upper troposphere, where $q_c \gg q_v^*$.

How, then, should the microphysical processes of fallout and evaporation be treated in our simple model? Clearly, these processes are too complicated to represent in any detail. Instead, we can represent the effect of those processes as a moistening of the environment. Since the net effect of radiation is to cause a cooling at each height in the free troposphere, there must be a net release of latent heat at each height in our model (recall that the updraft and its environment are at the same temperature, so sensible heat fluxes are prohibited). Therefore, the gross evaporation (the sum of all positive evaporation) must be less than the gross condensation (the sum of all positive condensation) at each height in the free troposphere. Let us denote the ratio of gross evaporation to gross condensation by α, which, in general, varies with height. Since the gross condensation is $[\gamma - \varepsilon(1 - \mathrm{RH})]Mq_v^*$ from Eq. (13), the gross evaporation is $\alpha[\gamma - \varepsilon(1 - \mathrm{RH})]Mq_v^*$.

Having defined α, we can account for condensates by modifying Eq. (21) to

$$-\partial_z q_v = \delta(q_v^* - q_v) + \alpha[\gamma - \varepsilon(1 - \mathrm{RH})]q_v^*. \quad (23)$$

Using the fact that $\partial_z q_v^* = -\gamma q_v^*$ and $q_v = \mathrm{RH}q_v^*$, and assuming the variations of RH with height are small (allowing us to drop the $\partial_z\mathrm{RH}$ term), this can be rewritten as

$$\mathrm{RH} = \frac{\delta + \alpha\gamma - \alpha\varepsilon}{\delta + \gamma - \alpha\varepsilon}. \quad (24)$$

Note that Eq. (12) is obtained from Eq. (24) by setting $\alpha = 0$. Thinking a bit about Eq. (24) reveals that α modifies RH quantitatively, but not in a qualitative way. Where the mass flux goes to zero at the top of the troposphere, δ goes to infinity, so RH goes to one, regardless of the value of α. Everywhere else δ is finite, so RH must still be less than one (since $\alpha < 1$, as required by the need for net latent heating at each height in the free troposphere). Furthermore, we can expect that α reinforces the C shape of the RH profile. By Eq. (24), a larger α favors a larger RH, and α is likely to be largest in the lower and upper troposphere, where there is shallow nonprecipitating convection and a large q_c/q_v^* ratio, respectively.

The bottom panels of Fig. 5 show the theoretical temperature and RH profiles for $\alpha = 0.5$, which can be compared with the top panels, which use $\alpha = 0$. The calculation of the $\alpha = 0.5$ profiles uses Eq. (24) for relative humidity and Eq. (B2) for the temperature lapse rate; the latter is derived in appendix B. As expected, the evaporation of condensates increases the relative humidity, but does not change its overall shape. As evidenced by the higher cold-point tropopause, the evaporation of condensates also decreases the lapse rate. In the limit of $\alpha = 1$ (i.e., zero net latent heat release), RH = 1 and the lapse rate reduces to the adiabatic value of $\Gamma = g(1 + q_v^*L/R_aT)/(c_p + q_v^*L^2/R_vT^2)$.

7. A lower bound on precipitation efficiency

We can use Eq. (24) to place a constraint on the precipitation efficiency that relies not on evaporation kinetics, free fall speeds, or any other detail of microphysics. The bound that we will derive here is a consequence solely of the atmospheric water budget. To begin, we must reassess Eq. (15), which gave the condition on the convective mass flux that must be

satisfied for moist convection to exist. In the derivation from section 2c, Eq. (13) for the condensation rate is unchanged by the addition of evaporation in the environment, so the inequality in Eq. (14) for RH is also unchanged. The expression for RH, however, does change; the new expression is given by Eq. (24). The new condition for the existence of moist convection is obtained by substituting Eq. (24) into Eq. (14). Through a seemingly miraculous cancellation of terms, this regenerates Eq. (15). So, even in the presence of hydrometeor evaporation, the requirement for moist convection to exist is $\partial_z M < \gamma M$, which is independent of α. Physically, this makes sense. When $\partial_z M = \gamma M$, there is no condensation in updrafts, so there are no hydrometeors to evaporate. Naturally, then, this upper bound on $\partial_z M$ does not depend on α.

Next, we can work with Eq. (24) to find a relationship between α and RH. Solving Eq. (24) for α, we get

$$\alpha = \text{RH} \frac{A}{B}, \tag{25}$$

where

$$A = \gamma - (1 - \text{RH}) \frac{\delta}{\text{RH}} \quad \text{and} \tag{26}$$

$$B = \gamma - (1 - \text{RH})\varepsilon. \tag{27}$$

Since α and RH are positive by definition, either A and B are both positive or both negative. To determine their sign, consider B. By Eq. (13), B is equal to the gross condensation rate c divided by the mass flux M and q_v^*, all of which are positive. Therefore, A and B are both positive.

Having established that both A and B are positive, Eq. (25) leads to a simple, but powerful, inequality. Since the convective mass flux generally decreases throughout the troposphere, δ is usually greater than ε, and, therefore, δ/RH is almost certainly greater than ε. Comparing Eqs. (26) and (27), this implies that $A < B$. Therefore, Eq. (25) implies that

$$\alpha < \text{RH}. \tag{28}$$

In other words, the ratio of gross evaporation to gross condensation is everywhere less than the relative humidity.

This, in turn, tells us something about the precipitation efficiency (PE). Let us define $\text{PE}(z)$ as the net condensation per area above height z divided by the gross condensation per area above height z. The gross condensation per volume is c and the net condensation per volume is $(1 - \alpha)c$. Therefore, the PE is given by

$$\text{PE}(z) = \frac{\int_z^\infty dz'(1 - \alpha)c}{\int_z^\infty dz'c}. \tag{29}$$

Using the fact that $\alpha < \text{RH}$, we can write $1 - \alpha > 1 - \text{RH}$ and

$$\text{PE}(z) > 1 - \frac{\int_z^\infty dz'\text{RH}c}{\int_z^\infty dz'c}. \tag{30}$$

The second term on the right-hand side is the mean RH of the atmosphere above z, weighted by the condensation rate, which decreases rapidly with height thanks to the exponential dependence of q_v^* on temperature. Therefore, we can approximate this term by $\text{RH}(z)$. So, we find that

$$\text{PE}(z) \gtrsim 1 - \text{RH}(z). \tag{31}$$

At the cloud base, where RH is around 0.8–0.9, this is not a very stringent constraint. Precipitation efficiencies reported by cloud-resolving simulations are around 25% (Pauluis and Held 2002; Romps 2011), and these include the evaporation of rain in the subcloud layer (implying that the precipitation efficiency at the cloud base is higher). Higher up in the troposphere, however, RH takes smaller values, so Eq. (31) places a more stringent bound.

The left panel of Fig. 9 plots the profiles of $1 - \text{RH}$ (dashed) and PE (solid) from the cloud-resolving simulation with a SST of 300 K. In agreement with Eq. (31), PE is greater than $1 - \text{RH}$ everywhere throughout the free troposphere. Furthermore, PE does not stray far from $1 - \text{RH}$, which is the expected behavior so long as δ/RH does not stray too far from ε. Like $1 - \text{RH}$, the profile of precipitation efficiency broadly resembles an inverted C, with low values of PE in the lower and upper troposphere, and a maximum of PE in the middle of the troposphere.

The right panels shows the convective mass flux M, defined as the horizontal and temporal average of $\rho w \mathcal{H}(q_c - 10^{-5})\mathcal{H}(w - w_0)$, where $\mathcal{H}$ is the Heaviside unit step function, q_c is the mass fraction of nonprecipitating condensates, w is vertical velocity, and $w_0 = 1\,\text{m s}^{-1}$. At the height where M goes to zero, the inequality breaks down. This is not unexpected: the inequality of $\text{PE} \gtrsim 1 - \text{RH}$ was derived for the convecting troposphere, so should not be expected to hold elsewhere. Indeed, we actually expect negative values of PE here since convective overshoots inject ice that then sublimates. In the convecting
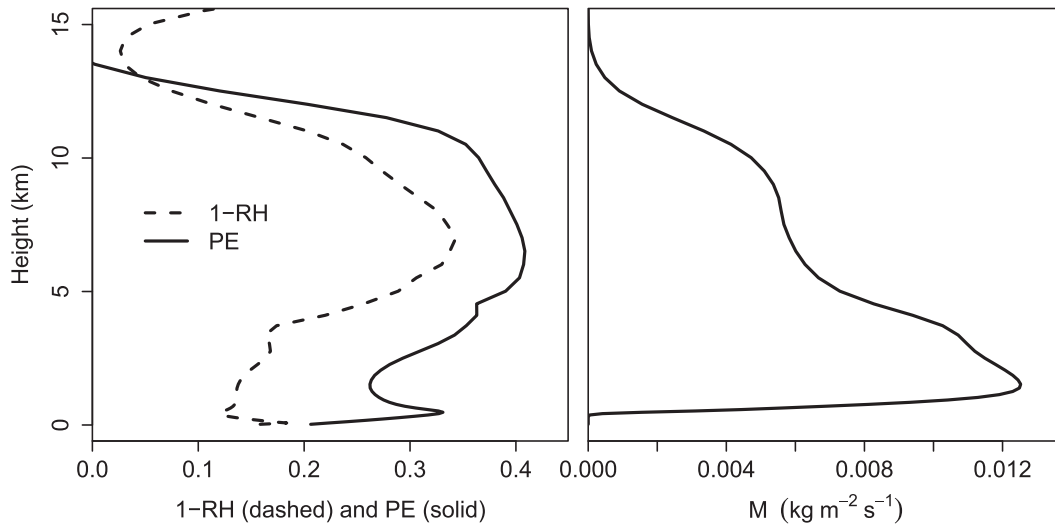
FIG. 9. (left) Profiles of $1 - \mathrm{RH}$ (dashed) and precipitation efficiency (solid) for a cloud-resolving simulation of RCE and (right) the profile of convective mass flux M for the same simulation. As predicted by the theory, $\mathrm{PE} > 1 - \mathrm{RH}$ throughout the convecting troposphere. See the text for the definition of precipitation efficiency.

troposphere, however, the lower bound on the precipitation efficiency is obeyed.

8. Discussion

A simple, analytical theory has been given here for the relative humidity in radiative–convective equilibrium, its changes with atmospheric warming, and its relationship to the precipitation efficiency. In particular, the theory has provided answers to the five questions posed in the introduction:

- (Section 3) The RH profile takes values in the range of 30%–90% because the length scale of subsidence drying (γ) is comparable to the length scale of convective moistening (δ). Since $\mathrm{RH} = \delta/(\delta + \gamma)$, RH cannot stray very far toward zero or one in the bulk of the troposphere. The one exception is the top of the troposphere where the mass flux goes to zero and, accordingly, the fractional detrainment rate δ goes to infinity. There, RH is one.

- (Section 4) The tropospheric RH profile is shaped like a "C" because of the height variations in the water-vapor lapse rate γ and the fractional detrainment rate δ. Since the temperature lapse rate Γ increases with height, γ also increases with height (i.e., the reduction in RH for a given amount of subsidence becomes greater the higher up you go). This increase in subsidence drying, aided by a decrease in convective moistening (i.e., $\partial_z \delta < 0$), causes RH to decrease with height in the lower troposphere. In the upper troposphere, however, the fractional detrainment rate increases rapidly as the convective mass flux dwindles,

and this convective moistening sends RH sailing back up toward unity at the top of the troposphere.

- (Section 5) For a fixed entrainment rate (FER) and fixed anvil temperature (FAT), the changes in RH with atmospheric warming are dictated by an invariant RH–T curve. These curves are calculated from the theory in the right panels of Fig. 6 for untuned sets of parameters and measured in cloud-resolving simulations in the right panels of Figs. 7 and 8. The point is not that the curves should be the same between the figures, but that the curve for a particular model (e.g., a particular cloud-resolving model or a particular global climate model) should be invariant under atmospheric warming. This greatly simplifies the task of predicting changes in the RH profile as a function of height or pressure. For example, if $\mathrm{RH} = 60\%$ and $T = 260\,\mathrm{K}$ at a height of 7 km in the current climate, then, in a warmer climate, a relative humidity of 60% can be found at whatever new height has a temperature of 260 K.

- (Section 6) The evaporation of hydrometeors tends to increase the relative humidity, as expected. Although this effect modifies the expression for RH from Eqs. (12)–(24), it does not alter the conclusions regarding the overall magnitude and shape of the RH profile. But, differences between microphysics schemes, which could affect the kinetics of precipitation evaporation, might explain the differences in the minimum RH between different cloud-resolving simulations. It is also conceivable that changes in precipitation efficiency with warming could alter the RH profile over the Indo-Pacific warm pool.

- (Section 7) The precipitation efficiency (PE) is found to be intimately related to the relative humidity. At each height, the ratio of evaporation to condensation (denoted by α) must be less than RH, which implies that α decreases with decreasing RH. Note that this is not a consequence of microphysical kinetics. In contrast, microphysics would likely require that α increase with decreasing RH since precipitation evaporates more rapidly in drier air. Instead, $\alpha <$ RH is a direct consequence of thermodynamics and the water budget, and it puts an increasingly stringent cap on α as RH decreases. Defining PE as the precipitation rate at height z divided by the integral of gross condensation above z, we can convert $\alpha <$ RH into a bound on the precipitation efficiency: PE $\gtrsim 1 -$ RH. In agreement with this bound, PE has a profile shaped like an inverted C with a maximum in the middle troposphere.

Recall that these conclusions stem from very basic physics: the Clausius–Clapeyron relation [Eq. (1)], hydrostatic balance [Eq. (4)], and the bulk-plume equations [Eqs. (7)–(9)].

It is instructive to consider how the theory presented here relates to the theory presented by SKR06, which is a simple example of an advection–condensation model. SKR06 assumes that an air parcel's RH decreases exponentially in time owing to subsidence drying and that the parcel is subject to Poisson-process saturation events with a time scale that is taken to be 7 days. The argument goes as follows. Assuming that the RH of a parcel decreases exponentially in time due to radiatively driven subsidence, we can write the time-dependent RH of the parcel as

$$\mathrm{RH} = e^{-t/\tau_d},$$

where the parcel is saturated at $t = 0$ and τ_d is a time scale that depends on the static stability and the radiative cooling rate. If the parcel is brought back to saturation in events that are distributed as a Poisson process, then the probability that a parcel is at time t from its last saturation is

$$p(t) = \frac{1}{\tau_m} e^{-t/\tau_m},$$

where τ_m is some tunable parameter (taken by SKR06 to be 7 days). Then, the probability distribution function (PDF) of RH can be found as

$$p(\mathrm{RH}) = \left| \frac{d\mathrm{RH}}{dt} \right|^{-1} p(t) = \frac{\tau_d}{\tau_m} \mathrm{RH}^{\tau_d/\tau_m - 1}. \qquad (32)$$

SKR06 presented evidence that the observed PDF of tropical RH could be described by a distribution of this form.

To compare the two theories, we must first calculate the mean RH predicted by Eq. (32). Denoting the mean relative humidity by RH, the theory of SKR06 would predict

$$\mathrm{RH} = \int_0^1 d\mathrm{RH}' p(\mathrm{RH}')\mathrm{RH}' = \frac{\tau_d}{\tau_d + \tau_m}. \qquad (33)$$

Note the resemblance between this and Eq. (12), which gives RH $= \delta/(\delta + \gamma)$. To make a connection between the two, we must first make physical sense of the SKR06 statement that τ_m is the time scale for a parcel to be moistened. This implies that a parcel is saturated in situ, which is unphysical if taken literally: in order for a parcel to become saturated, it must entrain into a convecting cloud, in which case it will likely rise. Nevertheless, we can justify the statement if we neglect the evaporation of hydrometeors and assume that the entrainment and detrainment rates are equal. In this case, we can think of τ_m as the time scale for a subsaturated parcel to be entrained and replaced by a detraining saturated parcel. If w is the speed of subsidence, then the time scale for this process would be $\tau_m = 1/(\delta w)$. Then, in this special case, Eq. (33) would reduce to Eq. (12) so long as $\tau_d = 1/(\gamma w)$. Equation (4) of SKR06 gives an expression for τ_d. Comparing it to this paper's Eq. (6), we see that SKR06 has omitted the pressure term (i.e., the $-g/R_a T$). This omission causes τ_d to be underestimated by about 30% in the lower tropical troposphere and about 10% in the tropical upper troposphere. Despite this difference, we have succeeded in making contact with the theory of SKR06. We conclude that the PDF of RH presented by SKR06 is applicable when there is no evaporation of hydrometeors (i.e., $\alpha = 0$) and the convective mass flux is constant with height (i.e., $\varepsilon = \delta$).

In general, we can make contact with the entire class of advection–condensation models by thinking about the time since last saturation. In the tropics, a parcel's relative humidity can be predicted from the radiative cooling rate and its time since last saturation. As discussed above, the mean time since last saturation—the τ_m—will equal $1/(\delta w)$. If $\delta = 0.5 \, \mathrm{km}^{-1}$ and $w = 3 \, \mathrm{mm \, s}^{-1}$ (i.e., a cooling rate of $\sim 1 \, \mathrm{K \, day}^{-1}$), then $1/(w\delta) = 8$ days. This agrees well with the choice of $\tau_m = 7$ days, which SKR06 used to obtain a good fit to observed relative humidity in the tropical troposphere.

Another topic to consider is whether the theory of section 2 can be used more broadly than just radiative–convective equilibrium. In particular, could it be used as a toy model of relative humidity for the entire tropics? First, it is important to recognize that the model predicts a single, mean value of the relative

humidity at each height. In the tropical free troposphere, there is a wide range of relative humidities ranging from nearly saturated to nearly unsaturated. Therefore, this toy model would be useful only to the extent that it is useful to know something about the mean RH. Assuming that this is of use, then the next consideration is whether the tropics can be treated as a closed system with changes in a parcel's relative humidity largely driven by diabatic subsidence. Studies of Lagrangian trajectories in GCMs suggest that this may not be the case (Galewsky et al. 2005; Dessler and Minschwaner 2007). Those studies find a significant amount of drying of subtropical air is caused by midlatitude eddies. Therefore, to account for this effect, it may be necessary to add a drying term to the rhs of Eq. (11). Finally, it is important to ask whether it is fair to apply the bulk-plume equations to the entire tropics. In the tropics, there is a large mean meridional gradient of relative humidity from the equatorial region to the subtropics. Deep convective updrafts are located primarily in the equatorial region, so they are not likely entraining air with the same humidity as the domainwide mean, as assumed in the bulk-plume equations. Fortunately, this is not an insurmountable problem. The entraining air can be thought of as a mixture of air that was very recently detrained (which has a vapor mass fraction equal to q_v^*) and air that is representative of the mean domain (which has a vapor mass fraction of q_v). Let us denote the ratio of the former to the latter by χ. Then, Eq. (10) gets modified to

$$\partial_z q_v^* = \varepsilon\{[\chi q_v^* + (1 - \chi)q_v] - q_v^*\} - c/M \qquad (34)$$

$$= [(1 - \chi)\varepsilon](q_v - q_v^*) - c/M, \qquad (35)$$

where $\varepsilon' = (1 - \chi)\varepsilon$ becomes the new effective entrainment rate. Similarly, Eq. (11) gets modified to use an effective detrainment rate of $\delta' = (1 - \chi)\delta$. The more insulated the convection is from the subtropics, either by meridional distance or weakness of mixing, the larger χ becomes and the smaller ε' and δ' become. Since RH = $\delta'/(\delta' + \gamma)$, the theory would predict a lower mean RH for the entire tropics than for radiative–convective equilibrium.

APPENDIX A

The Pressure Dependence of q_v^*

Examining Eq. (19) and the expressions for a_1, a_2, and a_3, we see that Γ is not entirely independent of temperature: it depends on q_v^*, which is a function of both temperature and pressure. Nevertheless, we can show that this pressure dependence is small. Consider the snippet of a temperature profile that is labeled "initial" in Fig. A1. It is plotted on axes of pressure and temperature. If the atmosphere warms by an amount dT at constant pressure here, then the temperature profile will shift to the curve labeled "final." At constant pressure, the fractional change in q_v^* is given by

$$\frac{q_v^*(B) - q_v^*(A)}{q_v^*(A)} = \frac{L}{R_v T^2} dT, \qquad (A1)$$

where the A and B correspond to the points labeled in Fig. A1. This gives a fractional change in q_v^* ranging from about 6% K^{-1} in the lower troposphere to about 15% K^{-1} in the upper troposphere. On the other hand, the fractional change in q_v^* at constant temperature is much smaller. The pressure change between A and C is given by

$$dp = -g\rho \, dz = -g\rho \frac{dT}{\Gamma} = -\frac{gp}{R_a T \Gamma} dT. \qquad (A2)$$

At constant temperature, the fractional change in q_v^* due to a change in pressure is

$$\left. \frac{dq_v^*}{q_v^*} \right|_T = -\frac{dp}{p}. \qquad (A3)$$

Therefore,

$$\frac{q_v^*(C) - q_v^*(A)}{q_v^*(A)} = \frac{g}{R_a T \Gamma} dT. \qquad (A4)$$

This gives a fractional change of about 2% K^{-1} throughout the troposphere (as we move upward in the troposphere, the decrease in T is roughly compensated by the increase in Γ). This is much smaller than the 6%–15% K^{-1} change in q_v^* at constant pressure, and explains why the pressure dependence of Γ is so small.
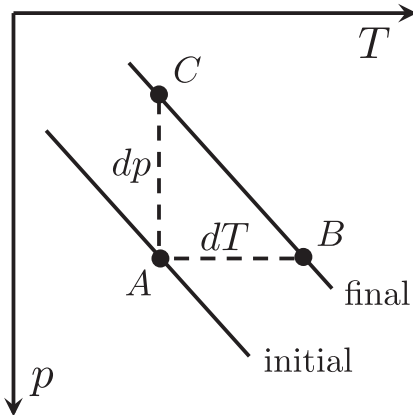
FIG. A1. A schematic illustrating a temperature profile that warms by dT at constant pressure. The change in q_v^* at constant pressure is given by $q_v^*(B) - q_v^*(A)$, while the change in q_v^* at constant temperature is given by $q_v^*(C) - q_v^*(A)$. By calculating these changes, we find that the changes in q_v^* at constant temperature are much smaller than those at constant pressure. See the text for details.

APPENDIX B

Lapse Rate for $\alpha \neq 0$

Section 2 derived Eqs. (12) and (19), which give expressions for the relative humidity and temperature lapse rate when there is no evaporation of condensates in the environment. As defined in section 6, α is the ratio of gross evaporation (in the environment) to the gross condensation (in the updrafts). When it is positive, Eq. (12) for the relative humidity gets replaced by the more general Eq. (24). Here, we will derive the generalization of Eq. (19) for the temperature lapse rate Γ in the case of positive α.

When $\alpha > 0$, there is no change to Eqs. (1)–(6), which simply embody the Clausius–Clapeyron relation and hydrostatic balance. Therefore, Eq. (16), which is derived from the definition of moist static energy and Eqs. (5)–(6), is unchanged. The vertical derivative of h^* in the updraft is still given by $\partial_z h^* = \varepsilon(h - h^*)$, where $h - h^* = L(q_v - q_v^*) = L(\mathrm{RH} - 1)q_v^*$, but RH is now given by Eq. (24), so Eq. (17) becomes

$$\partial_z h^* = -\varepsilon L q_v^* \frac{(1-\alpha)\gamma}{\delta + \gamma - \alpha\varepsilon}. \quad (B1)$$

Equating the right-hand sides of Eqs. (16) and (B1) and solving the quadratic equation, we find

$$\Gamma = \frac{R_v T^2}{L}\left(\frac{-b_2 + \sqrt{b_2^2 - 4b_1 b_3}}{2b_1} + \frac{g}{R_a T}\right), \quad (B2)$$

where

$$b_1 = \frac{R_v c_p T^2}{L} + q_v^* L,$$

$$b_2 = \frac{R_v c_p T^2}{L}\left(\delta - \alpha\varepsilon + \frac{g}{R_a T}\right) + q_v^* L(\delta - \varepsilon) - g, \quad \text{and}$$

$$b_3 = \left(\frac{R_v c_p T}{R_a L} - 1\right)g(\delta - \alpha\varepsilon).$$

Equations (24) and (B2) generalize Eqs. (12) and (19) to the case of nonzero α. These equations are used to generate the profiles in the bottom panels of Figs. 5 and 6.

REFERENCES

Arakawa, A., and W. H. Schubert, 1974: Interaction of a cumulus cloud ensemble with the large-scale environment, Part I. *J. Atmos. Sci.,* **31,** 674–701, doi:10.1175/1520-0469(1974)031<0674:IOACCE>2.0.CO;2.

Betts, A. K., 1990: Greenhouse warming and the tropical water budget. *Bull. Amer. Meteor. Soc.,* **71,** 1464–1465.

Böing, S. J., A. P. Siebesma, J. D. Korpershoek, and H. J. J. Jonker, 2012: Detrainment in deep convection. *Geophys. Res. Lett.,* **39,** L20816, doi:10.1029/2012GL053735.

Bretherton, C. S., P. N. Blossey, and M. Khairoutdinov, 2005: An energy-balance analysis of deep convective self-aggregation above uniform SST. *J. Atmos. Sci.,* **62,** 4273–4292, doi:10.1175/JAS3614.1.

Clough, S. A., M. W. Shephard, E. J. Mlawer, J. S. Delamere, M. J. Iacono, K. Cady-Pereira, S. Boukabara, and P. D. Brown, 2005: Atmospheric radiative transfer modeling: A summary of the AER codes. *J. Quant. Spectrosc. Radiat. Transfer,* **91,** 233–244, doi:10.1016/j.jqsrt.2004.05.058.

de Rooy, W. C., and Coauthors, 2013: Entrainment and detrainment in cumulus convection: An overview. *Quart. J. Roy. Meteor. Soc.,* **139,** 1–19, doi:10.1002/qj.1959.

Dessler, A. E., and K. Minschwaner, 2007: An analysis of the regulation of tropical tropospheric water vapor. *J. Geophys. Res.,* **112,** D10120, doi:10.1029/2006JD007683.

Fierro, A. O., E. J. Zipser, M. A. LeMone, J. M. Straka, and J. M. Simpson, 2012: Tropical oceanic hot towers: Need they be undilute to transport energy from the boundary layer to the upper troposphere effectively? An answer based on trajectory analysis of a simulation of a TOGA COARE convective system. *J. Atmos. Sci.,* **69,** 195–213, doi:10.1175/JAS-D-11-0147.1.

Folkins, I., K. Kelly, and E. Weinstock, 2002: A simple explanation for the increase in relative humidity between 11 and 14 km in the tropics. *J. Geophys. Res.,* **107,** 4736, doi:10.1029/2002JD002185.

Galewsky, J., A. Sobel, and I. Held, 2005: Diagnosis of subtropical humidity dynamics using tracers of last saturation. *J. Atmos. Sci.,* **62,** 3353–3367, doi:10.1175/JAS3533.1.

Harrop, B. E., and D. L. Hartmann, 2012: Testing the role of radiation in determining tropical cloud-top temperature. *J. Climate,* **25,** 5731–5747, doi:10.1175/JCLI-D-11-00445.1.

Hartmann, D., and K. Larson, 2002: An important constraint on tropical cloud-climate feedback. *Geophys. Res. Lett.,* **29,** 1951, doi:10.1029/2002GL015835.

Held, I. M., R. S. Hemler, and V. Ramaswamy, 1993: Radiative–convective equilibrium with explicit two-dimensional moist

convection. *J. Atmos. Sci.,* **50,** 3909–3927, doi:10.1175/1520-0469(1993)050<3909:RCEWET>2.0.CO;2.

Iacono, M. J., J. S. Delamere, E. J. Mlawer, M. W. Shephard, S. A. Clough, and W. D. Collins, 2008: Radiative forcing by long-lived greenhouse gases: Calculations with the AER radiative transfer models. *J. Geophys. Res.,* **113,** D13103, doi:10.1029/2008JD009944.

Krueger, S., Q. Fu, K. Liou, and H. Chin, 1995: Improvements of an ice-phase microphysics parameterization for use in numerical simulations of tropical convection. *J. Appl. Meteor.,* **34,** 281–287, doi:10.1175/1520-0450-34.1.281.

Kuang, Z., and C. S. Bretherton, 2006: A mass-flux scheme view of a high-resolution simulation of a transition from shallow to deep cumulus convection. *J. Atmos. Sci.,* **63,** 1895–1909, doi:10.1175/JAS3723.1.

——, and D. Hartmann, 2007: Testing the fixed anvil temperature hypothesis in a cloud-resolving model. *J. Climate,* **20,** 2051–2057, doi:10.1175/JCLI4124.1.

Lin, Y., R. Farley, and H. Orville, 1983: Bulk parameterization of the snow field in a cloud model. *J. Appl. Meteor.,* **22,** 1065–1092, doi:10.1175/1520-0450(1983)022<1065:BPOTSF>2.0.CO;2.

Lord, S., H. Willoughby, and J. Piotrowicz, 1984: Role of a parameterized ice-phase microphysics in an axisymmetric, nonhydrostatic tropical cyclone model. *J. Atmos. Sci.,* **41,** 2836–2848, doi:10.1175/1520-0469(1984)041<2836:ROAPIP>2.0.CO;2.

Malkus, J. S., 1952: The slopes of cumulus clouds in relation to external wind shear. *Quart. J. Roy. Meteor. Soc.,* **78,** 530–542, doi:10.1002/qj.49707833804.

Mapes, B. E., 2001: Water's two height scales: The moist adiabat and the radiative troposphere. *Quart. J. Roy. Meteor. Soc.,* **127,** 2353–2366, doi:10.1002/qj.49712757708.

Minschwaner, K., and A. E. Dessler, 2004: Water vapor feedback in the tropical upper troposphere: Model results and observations. *J. Climate,* **17,** 1272–1282, doi:10.1175/1520-0442(2004)017<1272:WVFITT>2.0.CO;2.

Paluch, I., 1979: The entrainment mechanism in Colorado cumuli. *J. Atmos. Sci.,* **36,** 2467–2478, doi:10.1175/1520-0469(1979)036<2467:TEMICC>2.0.CO;2.

Pauluis, O., and I. M. Held, 2002: Entropy budget of an atmosphere in radiative–convective equilibrium. Part I: Maximum work and frictional dissipation. *J. Atmos. Sci.,* **59,** 125–139, doi:10.1175/1520-0469(2002)059<0125:EBOAAI>2.0.CO;2.

Pierrehumbert, R. T., 1998: Lateral mixing as a source of subtropical water vapor. *Geophys. Res. Lett.,* **25,** 151–154, doi:10.1029/97GL03563.

——, H. Brogniez, and R. Roca, 2007: On the relative humidity of the atmosphere. *The Global Circulation of the Atmosphere,* T. Schneider and A. H. Sobel, Eds., Princeton University Press, 143–185.

Romps, D. M., 2008: The dry-entropy budget of a moist atmosphere. *J. Atmos. Sci.,* **65,** 3779–3799, doi:10.1175/2008JAS2679.1.

——, 2010: A direct measure of entrainment. *J. Atmos. Sci.,* **67,** 1908–1927, doi:10.1175/2010JAS3371.1.

——, 2011: Response of tropical precipitation to global warming. *J. Atmos. Sci.,* **68,** 123–138, doi:10.1175/2010JAS3542.1.

——, 2012: On the equivalence of two schemes for convective momentum transport. *J. Atmos. Sci.,* **69,** 3491–3500, doi:10.1175/JAS-D-12-068.1.

——, 2014: Rayleigh damping in the free troposphere. *J. Atmos. Sci.,* **71,** 553–565, doi:10.1175/JAS-D-13-062.1.

——, and Z. Kuang, 2010a: Do undiluted convective plumes exist in the upper tropical troposphere? *J. Atmos. Sci.,* **67,** 468–484, doi:10.1175/2009JAS3184.1.

——, and ——, 2010b: Nature versus nurture in shallow convection. *J. Atmos. Sci.,* **67,** 1655–1666, doi:10.1175/2009JAS3307.1.

Schneider, E. K., and R. S. Lindzen, 1976: A discussion of the parameterization of momentum exchange by cumulus convection. *J. Geophys. Res.,* **81,** 3158–3160, doi:10.1029/JC081i018p03158.

Sherwood, S. C., 1996: Maintenance of the free-tropospheric tropical water vapor distribution. Part II: Simulation by large-scale advection. *J. Climate,* **9,** 2919–2934, doi:10.1175/1520-0442(1996)009<2919:MOTFTT>2.0.CO;2.

——, E. R. Kursinski, and W. G. Read, 2006: A distribution law for free-tropospheric relative humidity. *J. Climate,* **19,** 6267–6277, doi:10.1175/JCLI3978.1.

——, W. Ingram, Y. Tsushima, M. Satoh, M. Roberts, P. L. Vidale, and P. A. O'Gorman, 2010a: Relative humidity changes in a warmer climate. *J. Geophys. Res.,* **115,** D09104, doi:10.1029/2009JD012585.

——, R. Roca, T. M. Weckwerth, and N. G. Andronova, 2010b: Tropospheric water vapor, convection, and climate. *Rev. Geophys.,* **48,** RG2001, doi:10.1029/2009RG000301.

Siebesma, A. P., and J. W. M. Cuijpers, 1995: Evaluation of parametric assumptions for shallow cumulus convection. *J. Atmos. Sci.,* **52,** 650–666, doi:10.1175/1520-0469(1995)052<0650:EOPAFS>2.0.CO;2.

Singh, M. S., and P. A. O'Gorman, 2013: Influence of entrainment on the thermal stratification in simulations of radiative-convective equilibrium. *Geophys. Res. Lett.,* **40,** 4398–4403, doi:10.1002/grl.50796.

Sun, D.-Z., and R. S. Lindzen, 1993: Distribution of tropical tropospheric water vapor. *J. Atmos. Sci.,* **50,** 1643–1660, doi:10.1175/1520-0469(1993)050<1643:DOTTWV>2.0.CO;2.

Tompkins, A., 2000: The impact of dimensionality on long-term cloud-resolving model simulations. *Mon. Wea. Rev.,* **128,** 1521–1535, doi:10.1175/1520-0493(2000)128<1521:TIODOL>2.0.CO;2.

Yang, H., and R. T. Pierrehumbert, 1994: Production of dry air by isentropic mixing. *J. Atmos. Sci.,* **51,** 3437–3454, doi:10.1175/1520-0469(1994)051<3437:PODABI>2.0.CO;2.